*Friction* **9**(5): 1110–1126 (2021)
https://doi.org/10.1007/s40544-020-0405-0
ISSN 2223-7690
CN 10-1237/TH
RESEARCH ARTICLE

# Combined effects of interface modification and micro-filler reinforcements on the thermal and tribological performances of fabric composites

**Junya YUAN[1], Zhaozhu ZHANG[1,2,*] Mingming YANG[1], Xin ZHAO[1], Liangfei WU[1,2], Peilong LI[1,2], Wei JIANG[1,*] Xuehu MEN[3], Weimin LIU[1]**

[1] *State Key Laboratory of Solid Lubrication, Lanzhou Institute of Chemical Physics, Chinese Academy of Sciences, Lanzhou 730000, China*

[2] *Center of Materials Science and Optoelectronics Engineering, University of Chinese Academy of Sciences, Beijing 100049, China*

[3] *School of Physical Science and Technology, Lanzhou University, Lanzhou 730000, China*

*Received: 02 March 2020 / Revised: 28 April 2020 / Accepted: 17 May 2020*



**Abstract:** The high specific-strength of glass fibers and exceptional self-lubrication of polytetrafluoroethylene (PTFE) fibers promote the potential application of hybrid PTFE/glass fabric composites in the tribological field, but their weak interfacial adhesion and inferior thermal properties significantly inhibit their tribological performance and reliability. Herein, a hybrid of polydopamine/silicon carbide/polyethyleneimine (PDA/SiC/PEI) functional coating was co-deposited onto the hybrid PTFE/glass fabric surface through a one-step impregnation method, leading to increased surface roughness and abundant amine groups. Tensile and peeling tests showed that this functional coating offered 47.8% enhancement in the fabric/matrix interfacial adhesion without compromising the strength of the pristine fabric. Moreover, the additional incorporation of $WS_2$, and aluminum nitride (AlN) micro-fillers contributed to the development of a high-quality tribofilm and improved the thermal properties of fabric composites. The results of wear tests proved that the hybrid-fabric composites, after the introduction of functional coating and micro-fillers, exhibited outstanding tribological performance, which was attributed to the superior interfacial adhesion as well as the synergistic enhancement effects between $WS_2$ and AlN micro-fillers.

**Keywords:** fabric; polymer composites; synergistic effect; friction and wear

## 1 Introduction

Fiber reinforced polymer (FRP) composites have attracted considerable attention in land vehicles, wind turbine blades, and aircraft because of their low-density, high specific strength/stiffness, outstanding fatigue/corrosion resistance, and excellent designability [1–6]. Hybrid-fabric composites are FRP composites with a unique weaving structure that allows them to integrate the unique performance advantages of different fibers to attain preferable and/or innovative properties [7, 8]. In particular, because of their well-known lubricating properties, polytetrafluoroethylene (PTFE) fibers, have emerged as excellent candidates to be blended with other high-performance reinforced fibers including glass fibers, carbon fibers, and aramid fibers for constructing self-lubricating liner material. Over the past years, our research group has carried out numerous related research studies on the tribological performance of the hybrid-fabric composite's design and considerable progress has been made [9–11]. Nevertheless, the weak interfacial adhesion between the fibers and the matrix, due to the low surface energy characteristics and smooth surfaces of PTFE and reinforced fibers,

* Corresponding authors: Zhaozhu ZHANG, E-mail: zzzhanglicp@yeah.net; Wei JIANG, E-mail: jiangwei@licp.cas.cn

remains a limiting factor in the improvement of the overall properties of the resulting fabric composites [12–14]. In addition, the poor thermal properties of most polymer matrices suggest that they cannot dissipate friction heat efficiently and provide effective carrying capacity at the sliding interfaces, further inhibiting their performance and reliability [15, 16].

Generally, in order to improve the interfacial adhesion strength between fibers and the polymer matrix of these composites to obtain satisfactory mechanical properties, most treatment methods aim to increase the fiber surface roughness and/or introduce specific functional groups in that are compatible with the polymer matrix. Based on by this, various surface modification techniques, including chemical vapor deposition (CVD), electrophoretic deposition (EPD), plasma etching, high-energy irradiation, chemical grafting, and polymeric sizing have been reported to change the surface structure and morphology of the fibers [17–23]. Modifications to the fiber surfaces can significantly improve the mechanical performance of FRP composites; however, maintaining the strength properties of the pristine fibers is still a major challenge. More importantly, these methods are not universally applicable and are largely restricted by the surface properties of the substrates. Therefore, developing an effective and versatile strategy for the surface modification of diverse materials has become a priority. Recently, mussel-inspired surface chemistry has gained attention owing to its versatility, simplicity, and widespread application [24–26]. Among these bio-based strategies for surface modification and functionalization, the polydopamine/polyethyleneimine (PDA/PEI) combinations exhibit a higher amine density, surface energy, and stability than combinations of pure polydopamine (PDA) and other non-covalent PDA co-deposited coatings [14, 27, 28]. Additionally, considering that the PDA/PEI can be co-deposited onto virtually all types of inorganic and organic materials and build functional coatings on their surfaces, nanomaterials and even micronmaterials can be introduced into the PDA/PEI reaction system and then simultaneously co-deposited with PDA/PEI onto fiber surfaces. The organic-inorganic hybrid functional coatings on fiber surfaces endow fibers with increased surface roughness and active functional groups, which enhance the interfacial adhesion properties of FRP composites. Furthermore, the entire co-deposition process takes place under mild reaction conditions and therefore does not significantly compromise the mechanical strength of the fibers.

In addition, to effectively solve the thermal dissipation problems at the sliding interface and to promote the load-carrying capability of FRP composites, a variety of micro-fillers have been incorporated to construct a heat conductive network in the matrix and to tailor the formation of a robust and uniform tribo-film on the counterface. Routinely, highly intrinsic thermally conductive fillers, such as aluminum nitrides (AlN), boron nitride (BN), carbon nanotubes (CNTs), and graphene oxide (GO), are incorporated into the polymer matrix to address the heat removal issues of composites [29–31]. Meanwhile, it has been noted that the introduction of solid lubricants, for example, graphite, graphitic carbon nitride (g-$C_3N_4$), $MoS_2$, and $WS_2$, into the polymer matrix contributes to the formation of solid lubricant tribofilms on the counterface owing to their layered structures [32–34]. Based on these by the above considerations, it is expected that the combination of thermally conductive fillers and solid lubricants can generate a synergetic effect hence improving the tribological performance of polymer composites.

To the best of our knowledge, there have been few studies investigating the effects of interface modification and microfiller reinforcement on the tribological behaviors of FRP composites. Herein, we develop a facile and scalable technique to improve the interfacial adhesion between hybrid PTFE/glass fabric and a phenolic resin matrix by co-depositing PDA/PEI with silicon carbide (SiC) nanoparticles onto fabric surfaces. Meanwhile, both the AlN and $WS_2$ micro-fillers were added to the hybrid-fabric composites to enhance the thermal properties and to contribute to the formation of a solid lubricant tribofilm. The surface microstructure and constitution of the SiC-coated hybrid fabric were analyzed. The mechanical and thermal performances of hybrid-fabric composites with SiC nanoparticles interfacial modification and AlN, $WS_2$ micro-filler reinforcements were also investigated. The tribological characteristics and internal wear mechanism of pristine and modified hybrid-fabric composites are discussed.

## 2 Experimental details

### 2.1 Reagents and materials

The hybrid PTFE/glass fabric (satin weave structure, $V_{PTFE}$:$V_{glass}$ = 3:1, area density of 420 g/m$^2$) was composed of low-friction PTFE fibers (DuPont Plant, USA) and high-strength glass fibers (Nanjing Fiberglass Research & Design Institute). A phenolic resin (resol) adhesive was obtained from Xing-Guang Chemical Reagent Plant. Dopamine hydrochloride (DA) and polyethylenimine (PEI, Mw = 600 Da) were purchased from Sigma-Aldrich and Meryer Chemical Tech. Co. Ltd., respectively. SiC (99.9%, 40 nm) nanoparticles were provided by Meryer Chemical Tech. Co. Ltd. AlN (99.5%, 2.0 μm) and $WS_2$ (99.9%, 2.0 μm) microfillers were supplied by Aladdin Biochemical Tech. Co. Ltd. The morphologies and spectra of the micro-fillers are shown in Fig. 1. All chemicals and solvents were used as received.

### 2.2 Preparation of SiC-coated hybrid PTFE/glass fabric

Prior to use, the hybrid PTFE/glass fabric was desized using petroleum ether and ethanol sequentially in a Soxhlet extractor and then dried at 50 °C. The surface modification of the hybrid fabric with SiC nanoparticles was performed using a one-step method based on dopamine chemistry, that is, co-deposition of DA, PEI, and SiC nanoparticles onto the hybrid PTFE/glass fabric. Typically, DA hydrochloride, PEI, and SiC nanoparticles were dissolved or dispersed in a Tris buffer solution (pH = 8.5, 20 mM) with a mass ratio of 2 : 2 : *X* (0.5, 1, 2) by intense ultrasonic treatment for 30 min. The concentrations of DA and PEI were fixed at 2 mg·mL$^{-1}$ in the solution, whereas the concentration of SiC nanoparticles was set to 0.5, 1, and 2 mg·mL$^{-1}$, respectively. The hybrid PTFE/glass fabric was subsequently immersed in the freshly prepared solution and gently stirred for 6 h at the ambient temperature. The resulting fabric sample, denoted as SiC@hybrid-fabric, was rinsed thoroughly with deionized water and dried overnight. Moreover, SiC@hybrid-fabrics with different concentrations of SiC nanoparticles (denoted as SiC@fabric-0.5, SiC@fabric-1, and SiC@fabric-2) were observed, and the optimal concentration conditions were confirmed. In addition, the SiC@hybrid-fabric was termed SiC@fabric-1 in the following text unless otherwise specified.

### 2.3 Fabrication of hybrid fabric/phenolic composites

The phenolic resin adhesive was first diluted with the

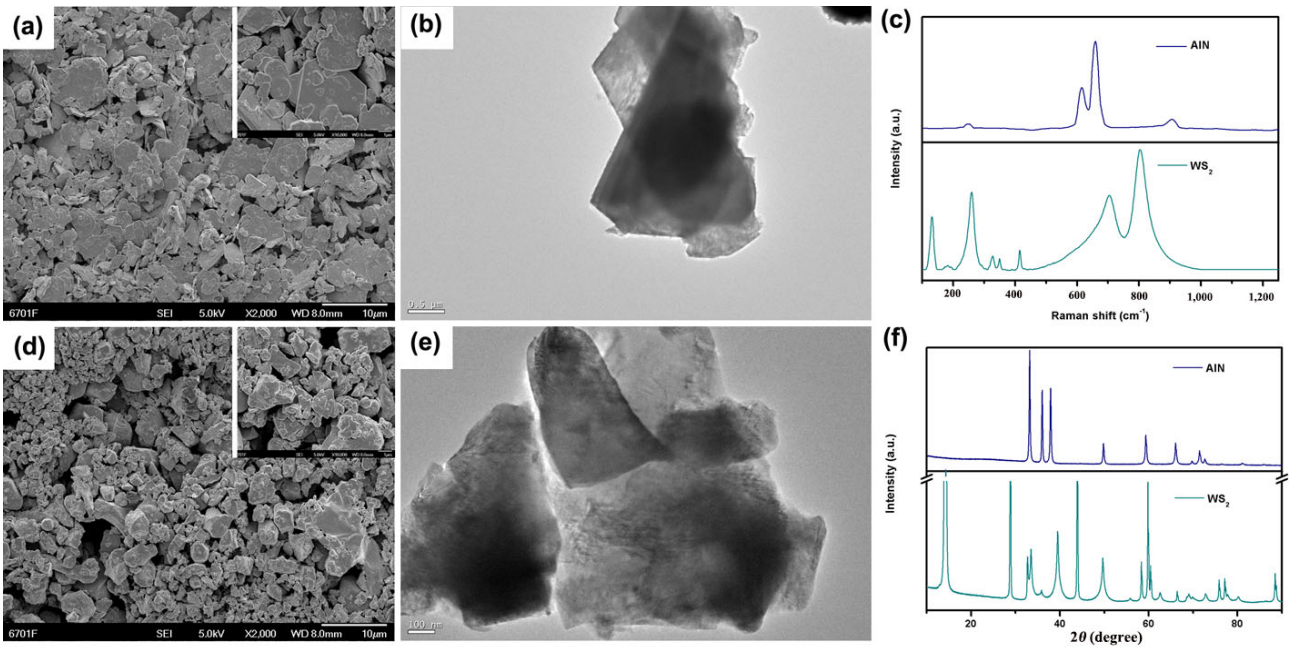


**Fig. 1** Scanning election microscopy (SEM) and transmission election microscopy (TEM) images of (a, b) $WS_2$ and (d, e) AlN micro-fillers, (c) Raman spectra and (f) XRD patterns of $WS_2$ and AlN micro-fillers.

mixed solvent ($V_{acetone}$: $V_{ethanol}$: $V_{ethyl\ acetate}$ = 1:1:1). The pre-calculated amounts of $WS_2$ (2 wt%), AlN (2 wt%), and mixed $WS_2$–AlN (1 wt%–1 wt%) micro-fillers were dispersed evenly in the phenolic resin solution by magnetic stirring and ultrasonic treatment to achieve a good dispersion of the fillers. Afterwards, the SiC@hybrid-fabric was immersed into the above-mentioned micro-fillers/phenolic resin adhesive solution. Repetitive immersion and drying of the hybrid PTFE/glass fabrics was performed until the weight fraction of the hybrid-fabrics reached 72% in the composites. The drying process was carried out at 50 °C for 10 min to remove the mixed solvent. Subsequently, the obtained prepregs were affixed onto the AISI-1045 steel disks using phenolic resin as an adhesive and then solidified at 180 °C for 2 h under 0.2 MPa. Moreover, pristine hybrid-fabric and SiC@hybrid-fabric composites were also prepared by a similar procedure in the absence of microfiller reinforcements to perform a control experiment. The typical preparation process of SiC@fabric/$WS_2$–AlN composites is illustrated in Fig. 2.

## 3 Results and discussion

### 3.1 Characterization of SiC@hybrid PTFE/glass fabric

Similar to the commonly known "bio-glue", PDA can deposit onto nearly all types of substrate surfaces, including smooth and chemically inert materials, and shows great potential for surface modification (Fig. S3 in the Electronic Supplementary Material (ESM)). Despite this, individual PDA deposition would generally lead to a rough coating resulting from the non-covalent stacking of large PDA aggregated particles [35]. Therefore, this method is still limited by inhomogeneous roughness, poor stability, inadequate surface wettability, and slow deposition rate. Thus, dopamine-assisted co-deposition strategies have attracted wide attention, because the surface properties of functional coatings can be easily adjusted by altering the molecular structure and content of co-deposited components. Therefore, the incorporation of polyethyleneimine (PEI) can efficiently destroy the non-covalent interactions of the PDA aggregated particles and accelerate the deposition process by Michael addition and Schiff-based reactions [36]. The resulting coating adheres to the substrate by electrostatic attractions, π-π stacking, and hydrogen bonding. In addition, inorganic nanomaterials can further be incorporated into the PDA/PEI co-deposition solution to design hybrid functional coatings, to combine the merits of inorganic nanomaterials and PDA/PEI copolymer coating as well as to generate synergistic effects between them. In this study, a PDA/SiC/PEI coating was co-deposited onto the hybrid PTFE/glass fabric surfaces to construct an organic-inorganic hybrid functional coating with different amounts of SiC nanoparticles. A recognized reaction mechanism is schematically presented in Fig. 3.

The surface morphologies of the pristine and modified glass and PTFE fibers characterized by field emission scanning electron microscopy (FESEM) are shown in Fig. 4. Clearly, it can be seen that the pristine glass and PTFE fiber surfaces are relatively neat and smooth, except for a few shallow striations along the fiber axis (Figs. 4(a) and 4(e)). In contrast, remarkable differences in the surfaces between the modified and pristine glass and PTFE fibers can be observed. Figures 4(b)–4(d) and Figs. 4(f)–4(h) show that the surface roughness of glass (PTFE) fibers increases significantly with the increased concentration of SiC nanoparticles. Therefore, SiC@Glass and SiC@PTFE

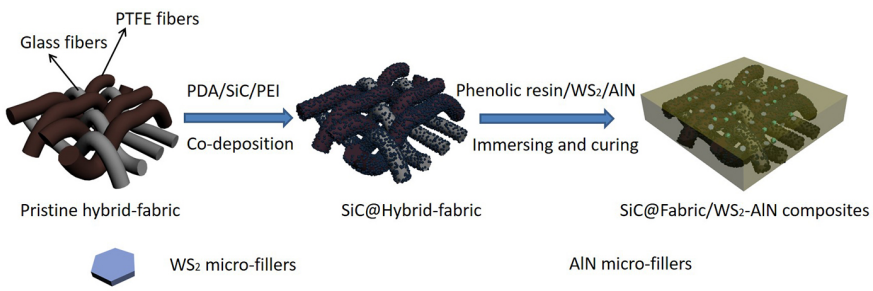


**Fig. 2** Schematic illustration of the preparation procedure for SiC@Fabric/$WS_2$–AlN composites.

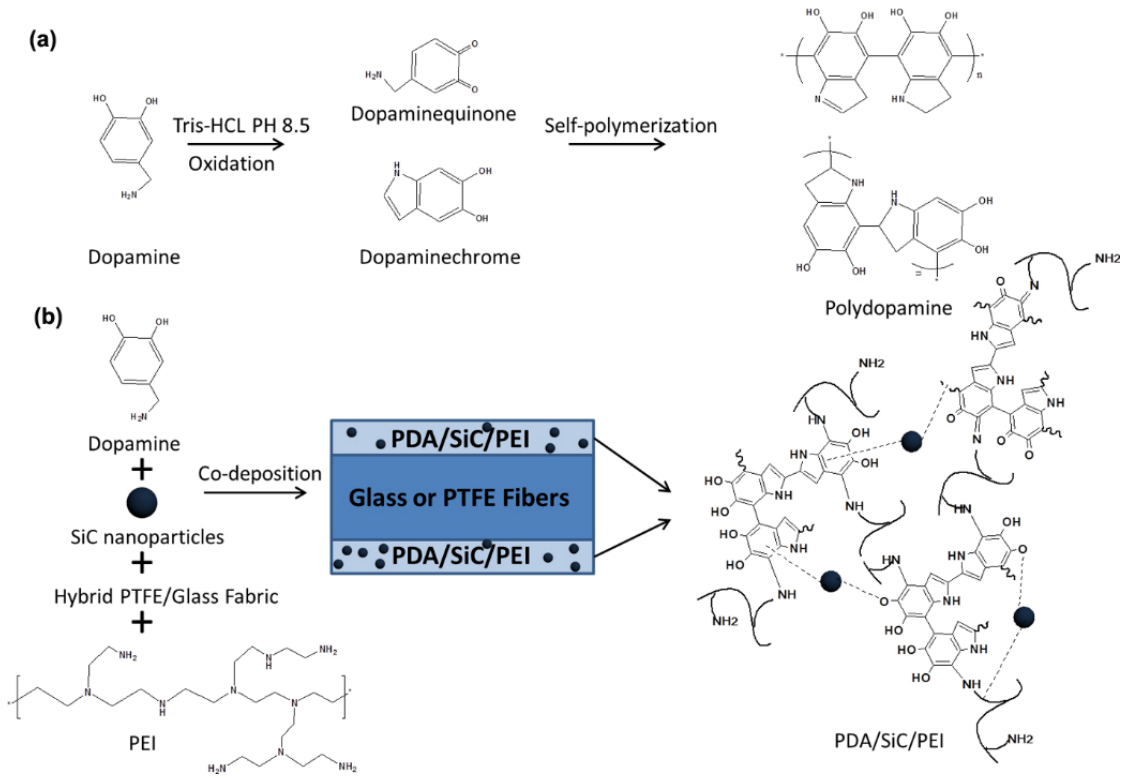


**Fig. 3** Schematic illustration of the possible reaction mechanism for (a) dopamine oxidative self-polymerization and (b) PDA/SiC/PEI co-deposited process.

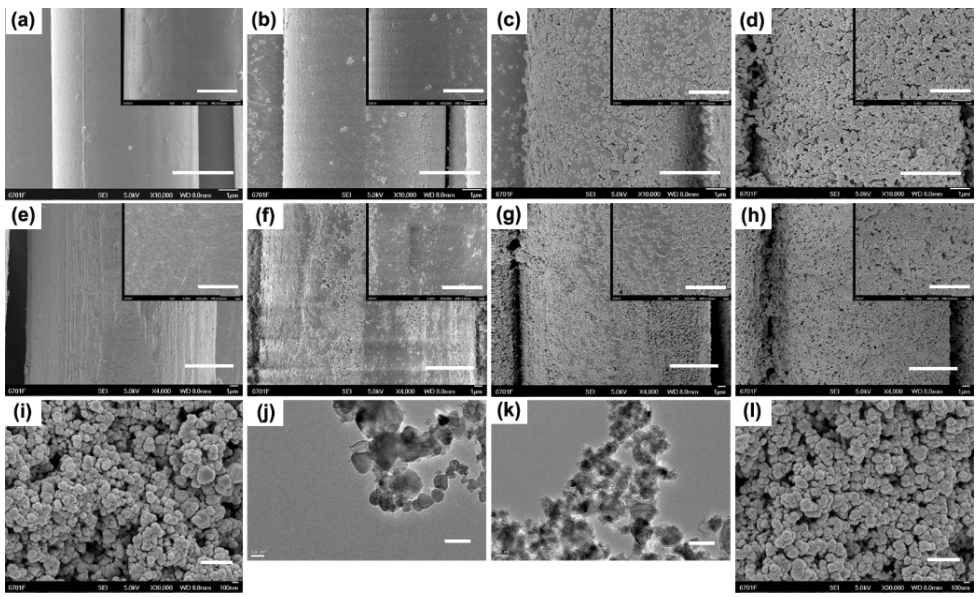


**Fig. 4** SEM images of the pristine (a, e), PDA/SiC/PEI coating with 0.5 (b, f), 1 (c, g), 2 mg·mL$^{-1}$ SiC nanoparticles (d, h) modified glass and PTFE fibers. The insets are the corresponding magnified images. SEM and TEM images of SiC (i, j) and SiC–PDA/PEI nanoparticles (l, k). Scale bars: (a–d) 3 μm, (e–h) 6 μm, (i, l) 500 nm, (j, k) 100 nm, and Agreeing strongly with this modification the insets of (a–h) 2μm.

fibers with 0.5 mg·mL$^{-1}$ SiC nanoparticles are shown in Figs. 4(b) and 4(f), respectively. The surface particles present a random dispersion and uneven distribution with obvious segregation. It can be presumed that the concentration of SiC nanoparticles is too low to satisfy the uniform spreading over the surfaces of the

hybrid PTFE/glass fabric. The surfaces of the SiC@glass and SiC@PTFE fibers with 1 mg·mL$^{-1}$ SiC nanoparticles exhibited uniform and dense nanoparticle arrangement (as shown in Figs. 4(c) and 4(g)). However, as the concentration of SiC nanoparticles increased to 2 mg·mL$^{-1}$, the surface particles of the hybrid PTFE/glass fabric showed significant aggregation and agglomeration suggesting that the SiC nanoparticles existing in the dopamine/PEI reaction system at this concentration also present the corresponding aggregation (as shown in Figs. 4(d) and 4(h)). The corresponding overall morphologies of the pristine and modified fibers are shown in Fig. S4 in the ESM. Moreover, in order to further examine the morphological features of SiC nanoparticles coated on hybrid PTFE/glass fabric surfaces, additional SEM and TEM characterization of SiC nanoparticles dispersed in the dopamine/PEI reaction solution without hybrid-fabric under the same conditions are shown in Figs. 4(k) and 4(l). It can be seen that the SiC nanoparticles are enwrapped uniformly by an ultrathin co-deposited coating. These results indicate that an organic-inorganic hybrid functional coating is co-deposited successfully onto the hybrid PTFE/glass fabric surfaces by this one-step method, and the amount of deposition can be regulated by varying the SiC nanoparticle concentration.

The surface chemical structure changes of SiC nanoparticles and hybrid PTFE/glass fabric are characterized by Fourier transform infrared spectroscopy (FTIR) spectra, as illustrated in Figs. 5(a) and 5(b). The virgin SiC nanoparticles have characteristic peaks at 1,085 and 890 cm$^{-1}$ assigned to the Si–O and Si–C stretching vibrations, respectively. New peaks arising at 3,240 cm$^{-1}$ and 1,440 cm$^{-1}$ after the PDA/PEI co-deposition process can be ascribed to the N–H and C–N stretching vibrations in the PDA/PEI coating. Furthermore, the presence of a broad peak at 1,600 cm$^{-1}$ illustrates the stretching of aromatic rings. In the spectra of the pristine hybrid PTFE/glass fabric, the signals at 1,200, 1,140, and 634 cm$^{-1}$ are associated with $CF_2$ stretching and rocking vibrations. In contrast, the SiC@hybrid-fabric exhibits a broader absorption peak at approximately 3,345 cm$^{-1}$, assigned to resonance vibration of $NH_2$ groups derived from PEI. Additionally, the absorption peaks observed at 2,920 and 2,860 cm$^{-1}$ represent the $CH_2$ stretching vibrations, and the peak at 890 cm$^{-1}$ is associated with the stretching vibration

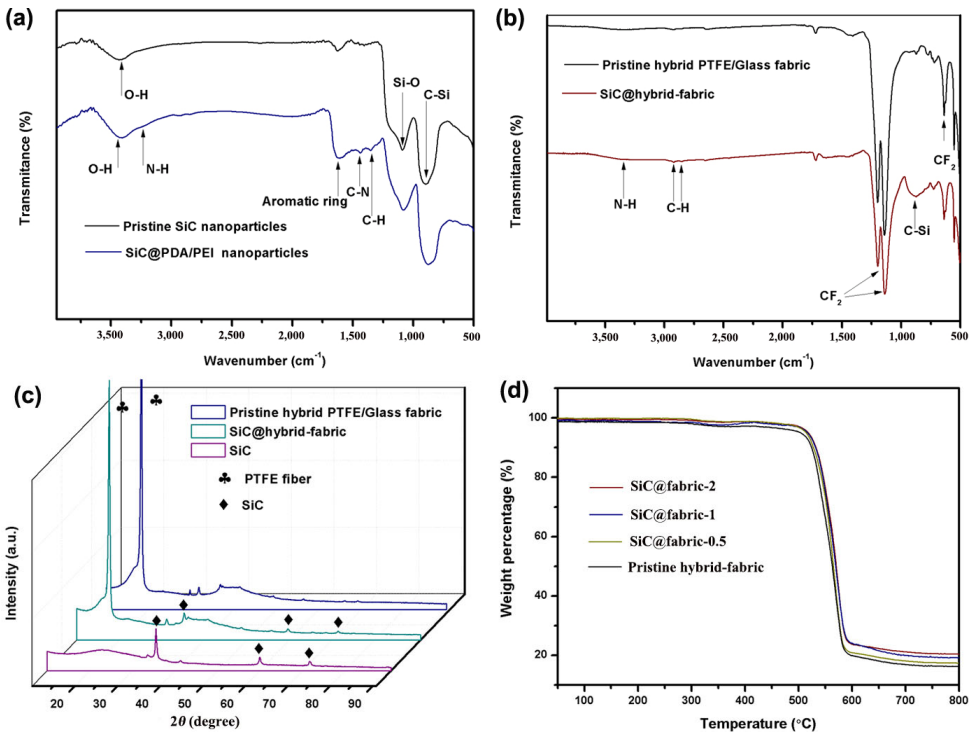


**Fig. 5** FTIR spectra of (a) SiC nanoparticles before and after PDA/PEI coating, (b–d) FTIR spectra, XRD patterns, and thermo gravimetric analysis (TGA) of the hybrid glass/PTFE fabric before and after co-deposition of PDA/SiC/PEI functional coating.

of Si–C. The XRD patterns of the hybrid PTFE/glass fabric before and after the co-deposition of the PDA/SiC/PEI coating are illustrated in Fig. 5(c). The diffraction peak appears at 18.0° assigned to the (100) crystalline plane of the PTFE fibers for the pristine hybrid PTFE/glass fabric. In the case of the SiC@hybrid-fabric, the new diffraction peaks at 35°, 60°, and 72° are assigned to the (111), (220), and (311) planes, respectively. Furthermore, thermogravimetric analysis was carried out in an oxygen atmosphere to ascertain the specific coating amount of SiC nanoparticles onto the hybrid-fabric surface (as shown in Fig. 5(d)). SiC nanoparticles and glass fibers have a high thermal stability with negligible mass loss up to 800 °C, whereas the PTFE fibers showed almost complete combustion at this temperature. Therefore, the SiC nanoparticle content on the hybrid-fabric surface could be determined from the residual weight at 800 °C. The residual weights for SiC@fabric-0.5, SiC@fabric-1, and SiC@fabric-2 at 800 °C were 17.3%, 19%, and 20.5%, respectively, attributed to the coating amount of SiC nanoparticles being 0.96%, 3.1%, and 5.03%, respectively.

XPS spectra were used to further examine the composition of the chemical elements and types of chemical bond of the hybrid PTFE/glass fabric and SiC nanoparticles, as shown in Fig. 6. The spectrum for the pristine glass fibers displays four peaks of Si 2p3/2, Si 2s, C 1s, and O 1s, whereas the new N 1s peak appears after the co-deposition of the PDA/SiC/PEI hybrid coating (Fig. 6(a)). In addition, the Si 2p3/2 peak in the SiC@glass fibers was resolved into

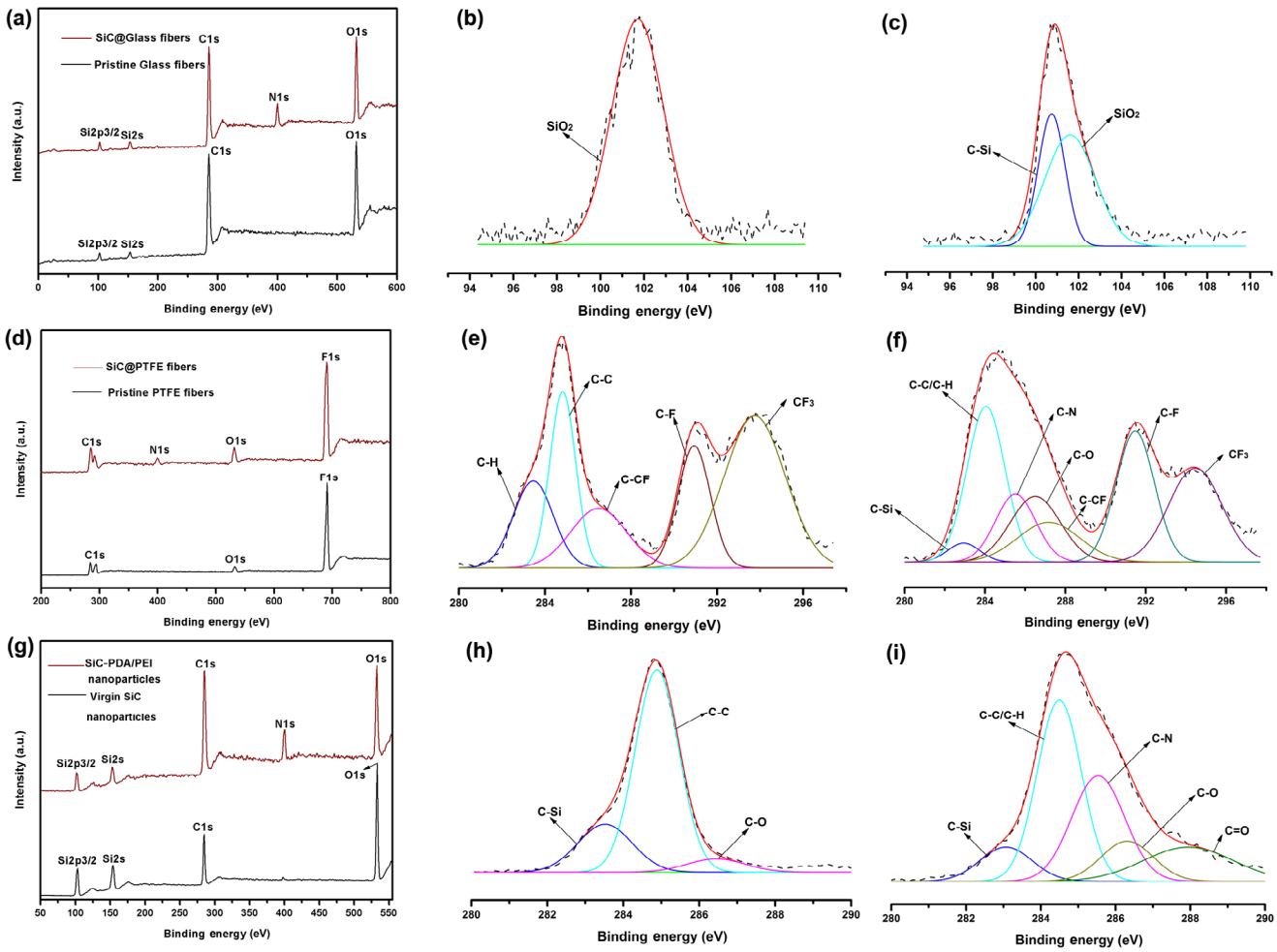


**Fig. 6** The survey scan spectra of (a) glass fibers, (d) PTFE fibers, and (g) SiC nanoparticles. The corresponding high-resolution Si 2p3/2 spectra of (b) pristine glass fibers and (c) SiC@glass fibers; the corresponding high-resolution C 1s spectra of (e) pristine PTFE fibers, (f) SiC@PTFE fibers, (h) virgin SiC nanoparticles, and (i) SiC–PDA/PEI nanoparticles.

C–Si (100.6 eV) and $SiO_2$ (101.8 eV), compared to the single $SiO_2$ bond type in pristine glass fibers. This is consistent with the chemical characteristics of the hybrid functional coating (Figs. 6(b) and 6(c)). For the SiC@PTFE fibers, an additional peak at 400 eV ascribed to N 1s appeared and the C/F ratio increased from 0.85 for pristine PTFE fibers to 1.36 (Fig. 6(d)). Meanwhile, the C 1s peak of pristine PTFE fibers could be divided into five peaks of C–H (283.4 eV), C–C (284.8 eV), C–CF (286.5 eV), C–F (290.9 eV), and $CF_3$ (293.8 eV), while the new C–Si (282.9 eV), C–N (285.5 eV), and C–O (286.6 eV) bands present in the C 1s peak of SiC@PTFE fibers, suggesting the successful co-deposition of PDA/SiC/PEI functional coating onto the surface of the PTFE fibers (Figs. 6(e) and 6(f)). Moreover, the emerging N element and additional C–N (285.5 eV), and C=O (288 eV) bands in the C 1s peak of SiC–PDA/PEI confirm the presence of the PDA/PEI coating on the surface of SiC nanoparticles (Figs. 6(g–i)).

### 3.2 Mechanical and thermal properties of hybrid PTFE/glass fabric composites

As discussed above, the coated PDA/SiC/PEI layer introduced significant surface roughness and substantial amine functional groups for the hybrid PTFE/glass fabric and thus provided numerous reactive sites for interfacial adhesion. The mechanical properties of the hybrid PTFE/glass fabric and their composites were evaluated by tensile and peeling tests to determine the interfacial properties and tensile strength of the hybrid-fabric, as shown in Fig. 7. In the case of SiC@fabric composites, the bonding strength reaches up to 3.4 N/mm, presenting a 47.8% increment compared to that of pristine fabric composites (2.3 N/mm). This remarkable increase can be attributed to the physical and chemical influences resulting from the PDA/SiC/PEI hybrid functional coating. First, an increase in the surface roughness of the hybrid-fabric will increase the interfacial contact area for resin infiltration and mechanical interlocking [37, 38]. On the other hand, the introduction of active functional groups onto the fabric surfaces allows the formation of chemical bonding between the fabric and resin matrix, thus leading to greatly improved interfacial adhesion [39]. Notably, the interfacial adhesion strength gradually decreases with a further increase in the SiC nanoparticle concentration, indicating that the agglomeration of SiC at the interphase degrades the interfacial adhesion of the fabric composites (Fig. S5 in the ESM). Excessive SiC nanoparticles can induce a local stress concentration and decrease the energy dissipation. In addition, the narrow gap between SiC can restrict the afflux of resin to the hybrid-fabric surface and result in poor interfacial adhesion between the fabric and phenolic resin. Comparable bonding strength was observed for the SiC@fabric/$WS_2$, SiC@fabric/AlN, and SiC@fabric/$WS_2$–AlN composites, suggesting that the introduction of $WS_2$, and AlN micro-fillers does not result in any discernible decrease in the interfacial adhesion of the fabric composites. Figure 7(b) shows the tensile strength results of pristine hybrid-fabric and SiC@hybrid-fabric are 400 and 380 N, respectively. It was found that the one-step co-deposition process does not cause serious degradation in the tensile strength of the hybrid PTFE/glass fabric,

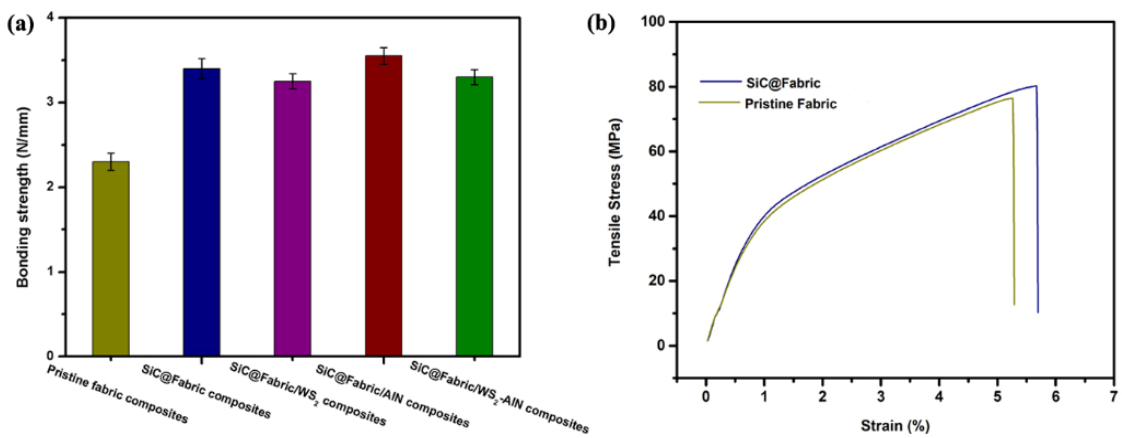


**Fig. 7** (a) The interfacial bonding strength of hybrid PTFE/glass fabric composites and (b) the tensile strength of hybrid-fabric.

due to the mild treatment conditions.

The change in bonding strength is closely related to the interfacial failure mode of fabric composites. Figure 8 depicts the surface morphology of the resin matrix after debonding from the reinforced fabric in the weft direction. Apparently, for the pristine fabric composites, it can be seen that the cambered surface of the phenolic resin is neat and regular implying that the debonding between the pristine fabric and resin matrix involves adhesive failure due to weak van der Waals forces. This phenomenon indicates that no resin fragments are attached to the fabric surface and the poor interfacial adhesion of pristine fabric composites. In contrast, the fracture surfaces of SiC@hybrid-fabric composites appear to become rough and abundant plastic dimples have emerged, suggesting the shift in the failure mode from adhesive failure involving fabric/matrix interfacial debonding to cohesive failure of the interphase. Meanwhile, the trace on the cambered surfaces of resin matrix from SiC@fabric/$WS_2$, SiC@fabric/AlN, and SiC@fabric/$WS_2$–AlN composites are not regular, consistent with the results shown in Fig. 7(a).

Under dry sliding, the temperature of the contact surface increased due to the accumulation of frictional heat, leading to the degradation of mechanical properties of the material resulting in a higher wear rate and friction failure [40, 41]. In consideration of the extreme temperature susceptibility of polymeric materials, thermal properties are therefore of great importance for the tribological performance of hybrid-fabric composites. The thermal stability of the pristine and modified hybrid PTFE/glass fabric composites was evaluated by TGA at a heating rate of 10 °C/min in air atmosphere. As seen in Fig. 9(a), all the samples displayed similar thermal degradation profiles within the temperature range, suggesting that the co-deposition of PDA/SiC/PEI functional coating and introduction of $WS_2$, and AlN micro-fillers did not significantly alter the degradation mechanism of the fabric composites. The pristine hybrid-fabric composites produced approximately 10 wt% weight residue due to the remaining glass fibers when heated to 600 °C, whereas the modified hybrid-fabric

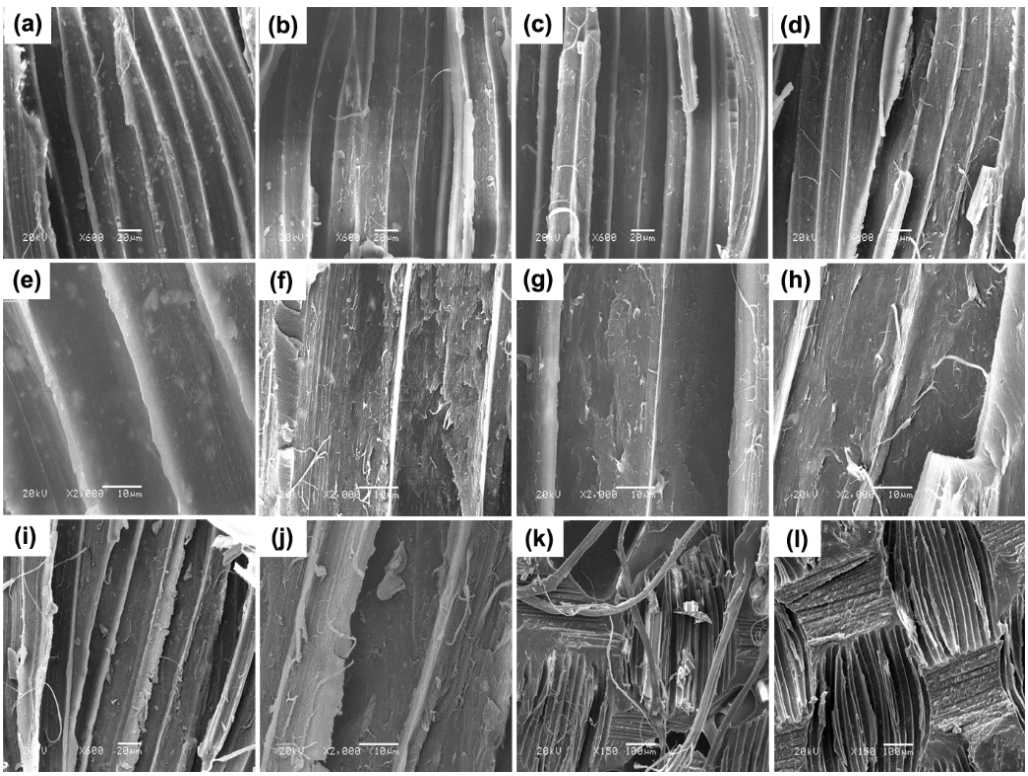


**Fig. 8** The fracture surfaces of hybrid-fabric composites after peeling tests: (a) Pristine fabric, (b) SiC@fabric, (c) SiC@fabric/$WS_2$, (d) SiC@fabric/AlN, (i) SiC@fabric/$WS_2$–AlN composites, (e–h, j) are the corresponding magnified images of (a–d, i), respectively, (k, l) are the overall images of (i) and (a).

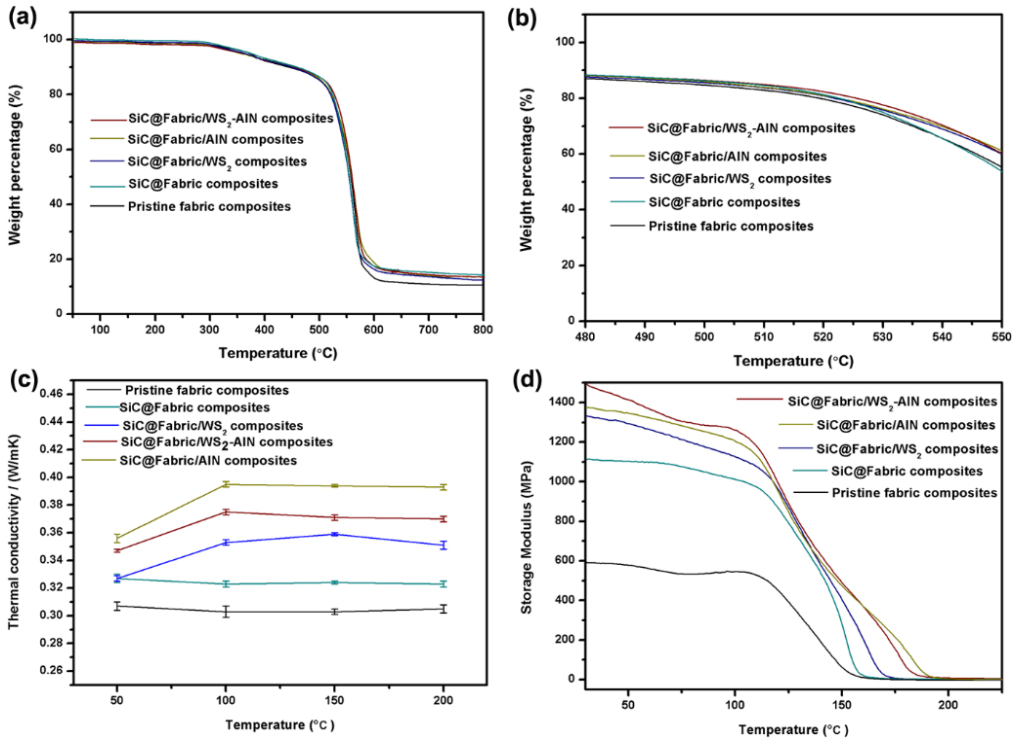


**Fig. 9** (a, b) TGA curves, (c) thermal conductivity, and (d) storage modulus of the pristine and modified hybrid PTFE/glass fabric composites.

composites exhibited a higher weight residual rate compared to that of the pristine fabric composites resulting from the introduction of SiC and AlN particles. From Table 1, it can be seen that both the $\overline{T}_{onset}$ and $\overline{T}_{max}$ of hybrid-fabric composites, after the introduction of the PDA/SiC/PEI functional coating, $WS_2$, and AlN micro-fillers, showed different levels of growth, indicative of the improvement of thermal stability. Specifically, the interface interaction between the SiC@hybrid-fabric and phenolic resin matrix can increase the thermal degradation activation energy of SiC@fabric composites by confining the thermal motion of the resin chains, thus improving the thermal stability of the phenolic resin [42]. Meanwhile, the additional $WS_2$ and AlN micro-fillers with high aspect ratios and specific surface areas in resin matrices construct a tortuous path for the diffusion of gaseous decomposition products and impedes the permeation rate of oxygen, leading to further improvement in the thermal stability of hybrid-fabric composites [43, 44].

Figure 9(c) shows the variations in the thermal conductivity ($K$) of the hybrid PTFE/glass fabric composites with increasing experimental temperature. Apparently, the $K$ value of pristine hybrid-fabric composites is maintained at approximately 0.30 W/mK that does not present significant alteration within the experimental temperature range. Moreover, a significant improvement in the $K$ value for the hybrid-fabric composites is observed with the co-deposition of hybrid functional coating and introduction of micro-filler reinforcements. For instance, the $K$ values of SiC@fabric, SiC@fabric/$WS_2$, SiC@fabric/$WS_2$–AlN, and SiC@fabric/AlN composites at 150 °C reached 0.324, 0.359, 0.371, and 0.394 W/mK, respectively, corres-

**Table 1** Results of $\overline{T}_{onset}$ and $\overline{T}_{max}$ of hybrid-fabric composites in oxygen atmosphere.

| Composite samples | Temperature | |
|---|---|---|
| | $\overline{T}_{onset}$ | $\overline{T}_{max}$ |
| Pristine fabric composites | 442.7 | 517 |
| SiC@fabric composites | 444.9 | 522.1 |
| SiC@fabric/$WS_2$ composites | 445.6 | 522.3 |
| SiC@fabric/AlN composites | 453 | 524 |
| SiC@fabric/$WS_2$–AlN composites | 453.5 | 525.2 |

Note: $\overline{T}_{onset}$ temperature corresponding to an average weight loss of 10 wt%;
$\overline{T}_{max}$ temperature corresponding to the average maximum rate of decomposition.

ponding to 8%, 19.6%, 23.6%, and 31.3% increment, respectively, in comparison to pristine hybrid-fabric composites. For the SiC@fabric composites, it is suggested that the interfacial thermal resistance between the hybrid-fabric and resin matrix is reduced by the co-deposition of the PDA/SiC/PEI functional coating that contributes to increasing the thermal conductivity. In addition, the introduction of $WS_2$ and AlN micro-fillers into hybrid-fabric composites further enhances the $K$ values that may be ascribed to the formation of additional thermally conductive pathways by bridging micro-fillers inside the resin matrix [45–47]. Meanwhile, the SiC@fabric/AlN composites present the highest $K$ value, resulting mainly from the improvement of interfacial adhesion and high intrinsic thermal conductivity of the AlN micro-fillers.

For examining the effects of the interfacial modification and $WS_2$–AlN micro-filler reinforcements on the storage modulus of the hybrid-fabric composites, the dynamic mechanical properties of the hybrid PTFE/glass fabric composites were measured by dynamic mechanical analysis (DMA), as shown in Fig. 9(d). It can be seen that the storage modulus of all hybrid-fabric composites decreases with increasing temperature. As the temperature increases, the components of the hybrid-fabric composites become much more mobile and start to move away from each other. Thus the stress transfer between the hybrid-fabric and resin matrix is heavily inhibited, resulting in a sharp decline in the storage modulus. Moreover, the storage modulus of the hybrid PTFE/glass fabric composites increased with the co-deposition of functional coating and introduction of micro-filler reinforcements. Specifically, the storage modulus at 30 °C was significantly enhanced from 600 MPa for the pristine fabric composites to 1,115 MPa for the SiC@fabric composites. This dramatic increase in the storage modulus indicates that the interfacial interactions between the SiC@hybrid-fabric and resin matrix are strong enough to ensure an effective load transfer to the hybrid-fabric, resulting in high mechanical strengths [48, 49]. Moreover, the $WS_2$–AlN micro-filler reinforcements within the resin matrix serve as the network centers to dissipate the local stress evenly and restrict the movements of the polymer chains, allowing a further increase in the stiffness of the hybrid PTFE/glass fabric composites.

### 3.3 Tribological properties of hybrid PTFE/glass fabric composites

The variations in the specific wear rates ($K_o$) and average friction coefficients ($\mu$) of the pristine and modified fabric composites subjected to different loading conditions are shown in Fig. 10. Clearly, the $K_o$ and $\mu$ of all hybrid-fabric composites increase markedly with increasing applied loads from 50 to 65 MPa, suggesting changes in the dominant wear mechanisms. The increase in friction force is normally undesirable for polymeric materials that not only accelerates the abrasion of the materials but also leads to a high contact temperature resulting from the friction heat, and thus a heat-inducible mechanical failure of the material. Under low loading conditions, the abrasion process of the hybrid PTFE/glass fabric generally undergoes fiber thinning, fiber fracture, and removal of broken pieces sequentially. However, as the

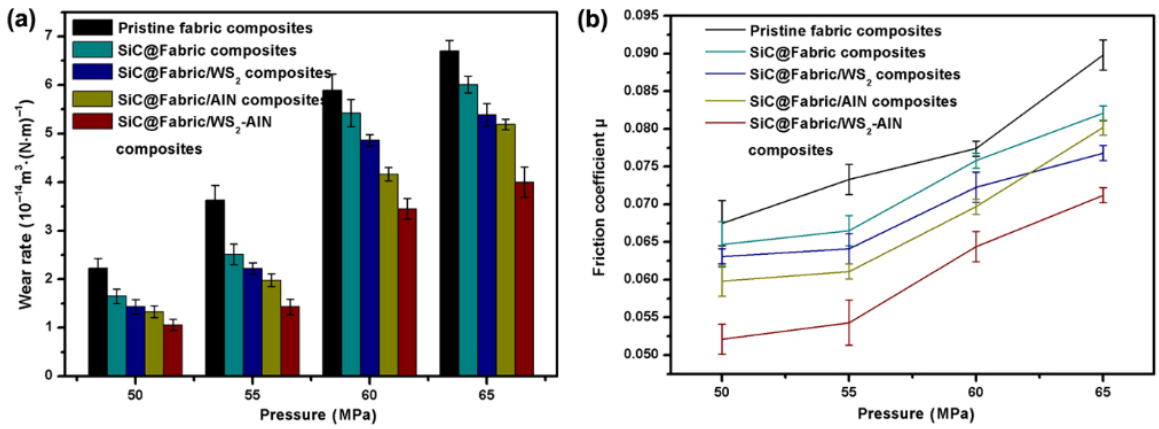


**Fig. 10** (a) Wear rate $K_o$ and (b) friction coefficient $\mu$ of pristine and modified hybrid PTFE/glass fabric composites (0.26 m/s, 120 min).

load increases, the breakage of the phenolic matrix occurs, especially at the fiber/matrix interfacial region; therefore, fiber bundles are cut off and pulled out more easily because of the lack of local support of the resin matrix. The resulting large fiber debris, especially the glass fiber debris, can further lower the abrasion resistance of the hybrid-fabric composites due to a third-body abrasive wear effect, resulting in the progressive increase of $K_o$ and $\mu$. Nevertheless, it can be seen that a satisfactory improvement in the tribological properties is achieved after the interfacial modification and introduction of $WS_2$–AlN micro-filler reinforcements under various applied loads. In the following sections, the wear mechanisms of hybrid-fabric composites are further investigated based on microscopic observations. In particular, the mechanisms for the positive effects of interfacial adhesion and micro-filler reinforcements on the tribological behaviors of hybrid-fabric composites are discussed in more detail.

Figure 11 compares the worn surfaces of the pristine and modified hybrid-fabric composites under dry-sliding conditions. Pristine fabric composites have been recognized for their severely worn surfaces, including resin peel-off, fiber breakage, debonding, and pull-out (Figs. 11(a) and 11(e)). These phenomena show that the internal reinforcing fibers are directly involved in the friction process without effective protection from the phenolic resin matrix, which can be ascribed to the resin adhesive on the fabric surface peeled off easily due to poor interfacial adhesion and resin degradation. As a result, a large amount of wear debris exists in the sliding interface and is distributed on the steel surface, as evidenced by the counterface morphology (Figs. 12(a) and 12(e)), generating a third-body abrasive wear effect accelerating the abrasion of pristine fabric composites consistent with the higher $K_o$ and $\mu$ values, as shown in Fig. 10. In contrast, the debonding and pull-out wear mechanism of the reinforced fibers were significantly alleviated for the SiC@fabric composites. Although resin exfoliation and some broken PTFE fibers still occur on the abrasion surface, the interior glass fibers are wrapped tightly by the phenolic resin and the dominant wear mechanism changes from fiber pull-out to fiber thinning. The improved fiber/matrix interfacial adhesion facilitates

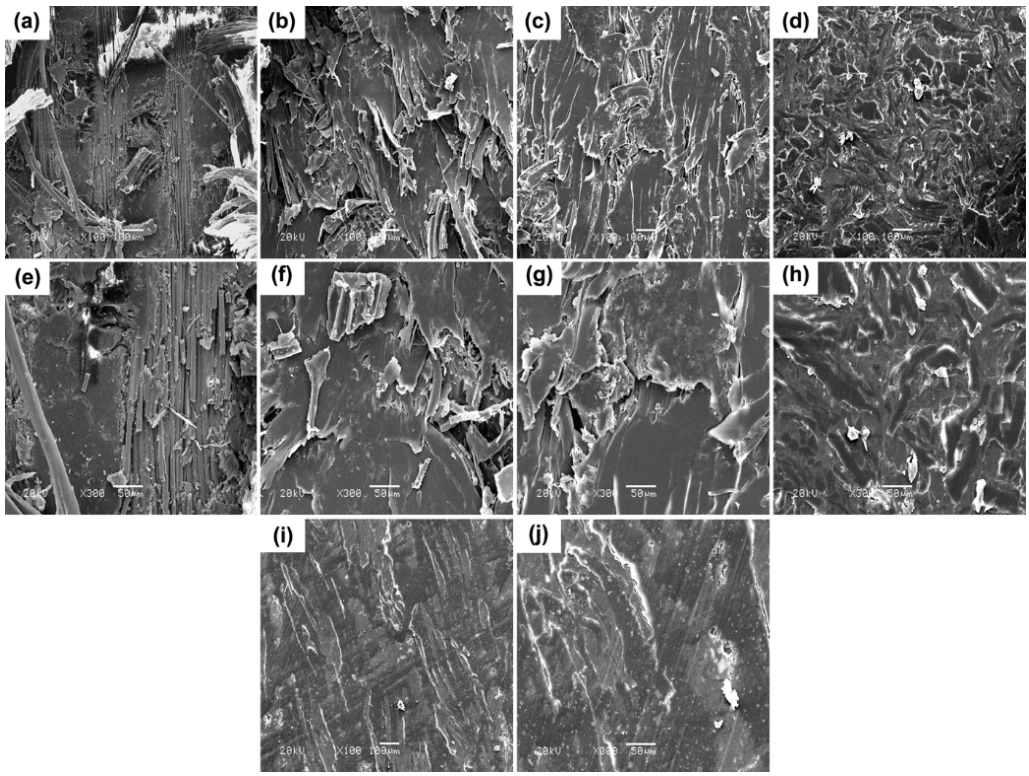


**Fig. 11** SEM images of the worn surfaces for (a) pristine, (b) SiC@Fabric, (c) SiC@Fabric/$WS_2$, (d) SiC@Fabric/AlN, and (i) SiC@Fabric/$WS_2$–AlN composites; (e–h, j) are the corresponding magnified images of (a–d, i), respectively, (55 MPa, 0.26 m/s, 120 min).

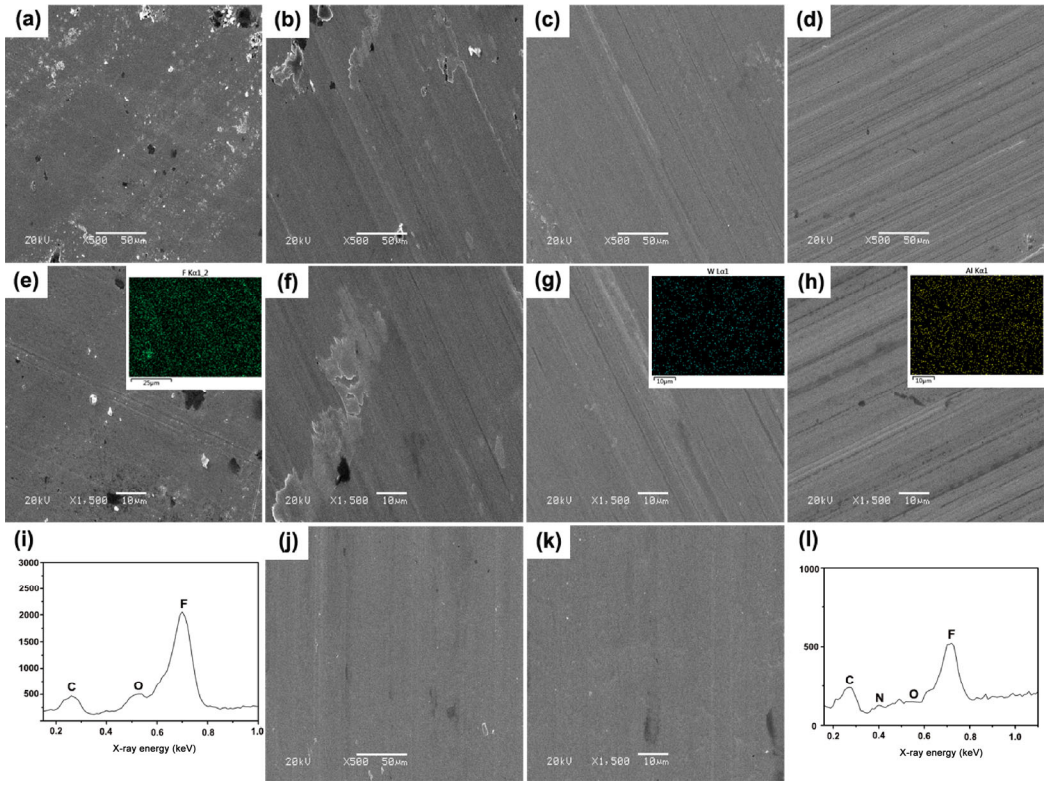


**Fig. 12** SEM images of the worn surfaces for counterface pins sliding against (a) pristine hybrid-fabric, (b) SiC@Fabric, (c) SiC@Fabric/$WS_2$, (d) SiC@Fabric/AlN, and (j) SiC@Fabric/$WS_2$–AlN composites (55 MPa, 0.26 m/s, 120 min); (e–h, k) are the corresponding magnified images of (a–d, j), respectively. The insets are the corresponding EDS images of F in (e), W in (g), and Al in (h); (i, l) are the corresponding EDS results of (e, k), respectively.

the absorption of rupture energy and realizes an effective stress transfer between the reinforced fabric and resin matrix. Thus the breakage of the matrix at the interfacial regions is much more limited, and the hybrid PTFE/glass fabric is always removed gradually accounting for the improved load-carrying capacity and reduced $K_o$ [50]. Further addition of low-loading micro-$WS_2$ into fabric composites leads to a much smoother worn surface and exerts an important influence on the transfer film structure (Table S1 in the ESM). In comparison to the patch-like tribofilm of SiC@fabric composites, a uniform, thin and continuous tribofilm is formed on the counterface surface after rubbing with SiC@fabric/$WS_2$ composites, implying that the beneficial role of micro-$WS_2$ in developing a high-quality tribofilm is responsible for the wear resistance of the fabric composites (Figs. 12(c) and 12(g)). Meanwhile, the incorporation of micro-AlN can effectively enhance the stiffness and creep resistance as well as the thermal conductivity of fabric composites that reduces the temperature increment in the contact area by dissipating the friction heat in a timely manner. As a result, the enhanced temperature resistance and cohesive strength of fabric composites resulted in improvements in wear resistance [51]. Compared to the addition of $WS_2$, and AlN micro-fillers, the addition of combined AlN–$WS_2$ reinforcements leads to an even smoother worn surface, where no serious fiber breakage and pull-out wear mechanism are characterized except for little phenolic resin exfoliation. Therefore, the lamellar micro-$WS_2$ contributes to producing a tough tribofilm withstanding severe rubbing conditions, while micro-AlN enhances the stiffness and cohesive strength of the resin matrix. Thus the synergistic effect between $WS_2$ and AlN leads to improved tribological properties of the fabric composites (Fig. S6 in the ESM). Based on the above results, a mechanism for the wear behavior of the hybrid PTFE/glass fabric composites as well as the synergistic effects between the PDA/SiC/PEI functional coating and $WS_2$, and AlN micro-fillers is shown in Fig. 13. Therefore, it is concluded that the combined interface

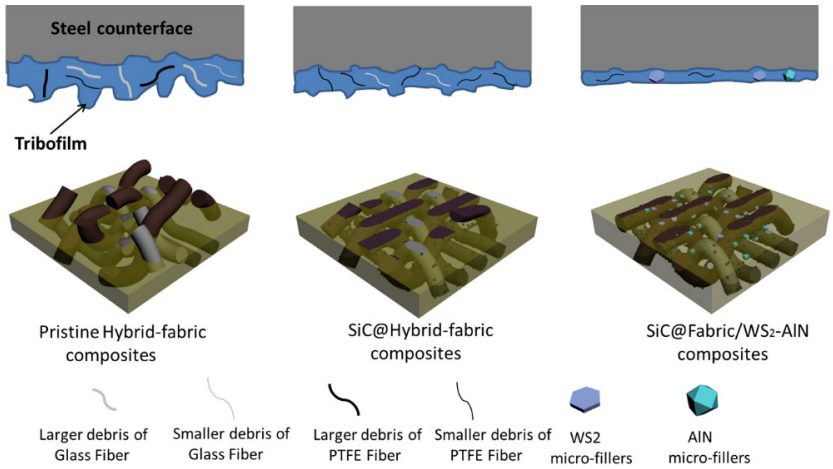


**Fig. 13** The schematic diagrams of wear mechanism for (a) pristine hybrid-fabric, (b) SiC@hybrid-fabric, and (c) SiC@fabric/$WS_2$–AlN composites.

modification and micro-filler reinforcements changes the wear mechanism of hybrid-fabric composites, leading to robust tribofilm, and improved thermal-mechanical properties.

## 4 Conclusions

In summary, a uniform and dense hybrid PDA/SiC/PEI layer was successfully coated onto the surface of a hybrid PTFE/glass fabric surface using a facile one-step co-deposition technique. The attachment of PDA/SiC/PEI was clearly verified to bring about increased surface roughness and more active functional groups for the hybrid-fabric that contributed to the improvement in interfacial adhesion through mechanical interlocking and chemical reaction. The improved fiber/matrix interfacial adhesion facilitates the absorption of rupture energy and leads to an effective stress transfer between the reinforced fabric and resin matrix during the sliding process. Meanwhile, the inclusion of the lamellar micro-$WS_2$ produces a tough tribofilm withstanding severe rubbing conditions, whereas micro-AlN enhances the stiffness and cohesive strength of the resin matrix. As a result, the SiC@fabric/$WS_2$–AlN composites exhibited optimal tribological performance under various applied loads.

## Acknowledgements

The authors gratefully acknowledge the financial support from the National Natural Science Foundation of China (Grant Nos. 51675252 and 51805516).

**Electronic Supplementary Material:** Supplementary material is available in the online version of this article at https://doi.org/10.1007/s40544-020-0405-0.



## References

[1] Yang X B, Jiang X, Huang Y D, Guo Z H, Shao L. Building nanoporous metal–organic frameworks "armor" on fibers for high–performance composite materials. *ACS Appl Mater Interfaces* **9**(6): 5590–5599 (2017)

[2] Hao B, Ma Q, Yang S D, Mäder E, Ma P C. Comparative study on monitoring structural damage in fiber–reinforced polymers using glass fibers with carbon nanotubes and graphene coating. *Compos Sci Technol* **129**: 38–45 (2016)

[3] Hung P Y, Lau K T, Cheng L K, Leng J S, Hui D. Impact response of hybrid carbon/glass fibre reinforced polymer composites designed for engineering applications. *Compos B Eng* **133**: 86–90 (2018)

[4] Zheng N, Huang Y D, Sun W F, Du X S, Liu H Y, Moody S, Gao J F, Mai Y W. *In–situ* pull–off of ZnO nanowire from carbon fiber and improvement of interlaminar toughness of hierarchical ZnO nanowire/carbon fiber hydrid composite laminates. *Carbon* **110**: 69–78 (2016)

[5] Siddiqui N A, Khan S U, Ma P C, Li C Y, Kim J K. Manufacturing and characterization of carbon fibre/epoxy composite prepregs containing carbon nanotubes. *Compos Part A: Appl Sci Manuf* **42**(10): 1412–1420 (2011)

[6] Yuan J Y, Zhang Z Z, Yang M M, Guo F, Men X H, Liu W M. Surface modification of hybrid–fabric composites with amino silane and polydopamine for enhanced mechanical and tribological behaviors. *Tribol Int* **107**: 10–17 (2017)

[7] Ren G N, Zhang Z Z, Song Y M, Li X M, Yan J Y, Wang Y Y, Zhu X T. Effect of MWCNTs–GO hybrids on tribological performance of hybrid PTFE/Nomex fabric/phenolic composite. *Compos Sci Technol* **146**: 155–160 (2017)

[8] Huang T, Li T S, Xin Y S, Liu P, Su C. Mechanical and tribological properties of hybrid fabric–modified polyetherimide composites. *Wear* **306**(1–2): 64–72 (2013)

[9] Yuan J Y, Zhang Z Z, Yang M M, Wu L F, Li P L, Guo F, Men X H, Liu W M. Coupling hybrid of BN nanosheets and carbon nanotubes to enhance the mechanical and tribological properties of fabric composites. *Compos Part A: Appl Sci Manuf* **123**: 132–140 (2019)

[10] Zhang Z Z, Yang M M, Yuan J Y, Guo F, Men X H. Friction and wear behaviors of $MoS_2$–multi–walled–carbonnanotube hybrid reinforced polyurethane composite coating. *Friction* **7**(4): 316–326 (2019)

[11] Su F H, Zhang Z Z, Guo F, Men X H, Liu W M. Friction and wear properties of fabric/phenolic composites with plasma treated–hybrid glass/PTFE fabric. *Compos Sci Technol* **67**(6): 981–988 (2007)

[12] Kim K, Jung Y C, Kim S Y, Yang B J, Kim J. Adhesion enhancement and damage protection for carbon fiber–reinforced polymer (CFRP) composites via silica particle coating. *Compos Part A: Appl Sci Manuf* **109**: 105–114 (2018)

[13] Lin J W, Xu P, Wang L L, Sun Y H, Ge X, Li G, Yang X P. Multi–scale interphase construction of self–assembly naphthalenediimide/multi–wall carbon nanotube and enhanced interfacial properties of high–modulus carbon fiber composites. *Compos Sci Technol* **184**: 107855 (2019)

[14] Liu Y, Fang Y C, Liu X L, Wang X L, Yang B. Mussel–inspired modification of carbon fiber via polyethyleneimine/polydopamine co–deposition for the improved interfacial adhesion. *Compos Sci Technol* **151**: 164–173 (2017)

[15] Meng H, Sui G X, Xie G Y, Yang R. Friction and wear behavior of carbon nanotubes reinforced polyamide 6 composites under dry sliding and water lubricated condition. *Compos Sci Technol* **69**(5): 606–611 (2009)

[16] Mao K. A numerical method for polymer composite gear flash temperature prediction. *Wear* **262**(11–12): 1321–1329 (2007)

[17] Yang M M, Zhang Z Z, Yuan J Y, Wu L F, Zhao X, Guo F, Men X H, Liu W M. Fabrication of PTFE/Nomex fabric/phenolic composites using a layer–by–layer self–assembly method for tribology field application. *Friction* **8**(2): 335–342 (2020)

[18] Li N, Zong L S, Wu Z Q, Liu C, Wang X, Bao F, Wang J Y, Jian X G. Amino–terminated nitrogen–rich layer to improve the interlaminar shear strength between carbon fiber and a thermoplastic matrix. *Compos Part A: App Sci Manuf* **101**: 490 – 499 (2017)

[19] Seghini M C, Touchard F, Sarasini F, Cech V, Chocinski–Arnault L, Mellier D, Tirillò J, Bracciale M P, Zvonek M. Engineering the interfacial adhesion in basalt/epoxy composites by plasma polymerization. *Compos Part A: Appl Sci Manuf* **122**: 67–76 (2019)

[20] Sun J F, Zhao F, Yao Y, Jin Z, Liu X, Huang Y D. High efficient and continuous surface modification of carbon fibers with improved tensile strength and interfacial adhesion. *Appl Surf Sci* 4**12**: 424–435 (2017)

[21] Yao X M, Gao X Y, Jiang J J, Xu C M, Deng C, Wang J B. Comparison of carbon nanotubes and graphene oxide coated carbon fiber for improving the interfacial properties of carbon fiber/epoxy composites. *Compos Part B: Eng* **132**: 170–177 (2018)

[22] Zhao M, Meng L H, Ma L C, Wu G S, Xie F, Ma L N, Wang W, Jiang B, Huang Y D. Stepwise growth of melamine–based dendrimers onto carbon fibers and the effects on interfacial properties of epoxy composites. *Compos Sci Technol* **138**: 144–150 (2017)

[23] Yang J, Chen Y, Xu P, Li Y, Jia X H, Song H J. Fabrication of compressible and underwater superoleophobic carbon/g–$C_3N_4$ aerogel for wastewater purification. *Mater Lett* **254**: 210–213 (2019)

[24] He G S, Liu J H, Gong F Y, Lin C M, Yang Z J. Bioinspired mechanical and thermal conductivity reinforcement of highly

explosive–filled polymer composites. *Compos Part A: Appl Sci Manuf* **107**: 1–9 (2018)

[25] Sa R N, Yan Y, Wei Z H, Zhang L Q, Wang W C, Tian M. Surface modification of aramid fibers by bio–inspired poly(dopamine) and epoxy functionalized silane grafting. *ACS Appl Mater Interfaces* **6**(23): 21730–21738 (2014)

[26] Shao Q, Hu Z, Xu X R, Yu L, Zhang D Y, Huang Y D. Mussel–inspired immobilization of BN nanosheets onto poly(p–phenylene benzobisoxazole) fibers: Multifunctional interface for photothermal self–healing. *Appl Surf Sci* **440**: 1159–1165 (2018)

[27] Lv Y, Du Y, Qiu W Z, Xu Z K. Nanocomposite membranes via the codeposition of polydopamine/polyethylenimine with silica nanoparticles for enhanced mechanical strength and high water permeability. *ACS Appl Mater Interfaces* **9**(3): 2966–2972 (2017)

[28] Wang J, Zhu J Y, Tsehaye M T, Li J, Dong G Y, Yuan S S, Li X, Zhang Y T, Liu J D, Van Der Bruggen B. High flux electroneutral loose nanofiltration membranes based on rapid deposition of polydopamine/polyethyleneimine. *J Mater Chem A* **5**(28): 14847-14857 (2017)

[29] Rathaur A S, Katiyar J K, Patel V K. Thermo–mechanical and tribological properties of SU–8/h–BN composite with SN150/perfluoropolyether filler. *Friction* **8**(1): 151–163 (2020)

[30] Muratov D S, Kuznetsov D V, Il'inykh I A, Burmistrov I N, Mazov I N. Thermal conductivity of polypropylene composites filled with silane–modified hexagonal BN. *Compos Sci Technol* **111**: 40–43 (2015)

[31] Ruan K P, Guo Y Q, Tang Y S, Zhang Y L, Zhang J N, He M K, Kong J, Gu J W. Improved thermal conductivities in polystyrene nanocomposites by incorporating thermal reduced graphene oxide *via* electrospinning–hot press technique. *Compos Commun* **10**: 68–72 (2018)

[32] Li H L, Zeng F P, Yin Z W, Jiang D, Huo Y J. A study on the tribological behavior of hybrid PTFE/Kevlar fabric composites filled with nano–SiC and/or submicron–$WS_2$ fillers. *Polymer Compos* **37**(7): 2218–2226 (2016)

[33] Wu L F, Zhang Z Z, Yang M M, Yuan J Y, Li P L, Guo F, Men X H. One–step synthesis of g–$C_3N_4$ nanosheets to improve tribological properties of phenolic coating. *Tribol Int* **132**: 221–227 (2019)

[34] Guo W L, Yin J, Qiu H, Guo Y F, Wu H R, Xue M M. Friction of low–dimensional nanomaterial systems. *Friction* **2**(3): 209–225 (2014)

[35] Qiu W Z, Yang H C, Xu Z K. Dopamine–assisted co–deposition: An emerging and promising strategy for surface modification. *Adv Colloid Interface Sci* **256**: 111–125 (2018)

[36] Pi J K, Yang H C, Wan L S, Wu J, Xu Z K. Polypropylene microfiltration membranes modified with $TiO_2$ nanoparticles for surface wettability and antifouling property. *J Membr Sci* **500**: 8–15 (2016)

[37] Dong J D, Jia C Y, Wang M Q, Fang X J, Wei H W, Xie H Q, Zhang T, He J M, Jiang Z X, Huang Y D. Improved mechanical properties of carbon fiber–reinforced epoxy composites by growing carbon black on carbon fiber surface. *Compos Sci Technol* **149**: 75–80 (2017)

[38] Yuan J Y, Zhang Z Z, Yang M M, Wang W J, Men X H, Liu W M. POSS grafted hybrid–fabric composites with a biomimic middle layer for simultaneously improved UV resistance and tribological properties. *Compos Sci Technol* **160**: 69–78 (2018)

[39] Sahin M, Schlögl S, Kalinka G, Wang J P, Kaynak B, Mühlbacher I, Ziegler W, Kern W, Grützmacher H. Tailoring the interfaces in glass fiber–reinforced photopolymer composites. *Polymer* **141**: 221–231 (2018)

[40] Meng Y, Su F H, Chen Y Z. Effective lubricant additive of nano–Ag/MWCNTs nanocomposite produced by supercritical $CO_2$ synthesis. *Tribol Int* **118**: 180–188 (2018)

[41] Luo W, Liu Q, Li Y, Zhou S T, Zou H W, Liang M. Enhanced mechanical and tribological properties in polyphenylene sulfide/polytetrafluoroethylene composites reinforced by short carbon fiber. *Compos Part B: Eng* **91**: 579–588 (2016)

[42] Guan Y, Li W, Zhang Y L, Shi Z Q, Tan J, Wang F, Wang Y H. Aramid nanofibers and poly (vinyl alcohol) nanocomposites for ideal combination of strength and toughness via hydrogen bonding interactions. *Compos Sci Technol* **144**: 193–201 (2017)

[43] Chen Z Y, Guo L L, Yan H X, Yao H H, Li L, Liu Q. Amino functionalization of graphene/graphene–like $MoSe_2$ hybrids as lubricant additives for bismaleimide composites: Preparation, mechanical and tribological properties. *Compos Part B: Eng* **161**: 263–271 (2019)

[44] Su Z, Wang H, Ye X Z, Tian K H, Huang W Q, He J, Guo Y L, Tian X Y. Anisotropic thermally conductive flexible polymer composites filled with hexagonal born nitride (h–BN) platelets and ammine carbon nanotubes (CNT–$NH_2$): Effects of the filler distribution and orientation. *Compos Part A: Appl Sci Manuf* **109**: 402–412 (2018)

[45] Chen C, Qiu S H, Cui M J, Qin S, Yan G P, Zhao H C, Wang L P, Xue Q J. Achieving high performance corrosion and wear resistant epoxy coatings via incorporation of noncovalent functionalized graphene. *Carbon* **114**: 356–366 (2017)

[46] Guo Y Q, Lyu Z Y, Yang X T, Lu Y J, Ruan K P, Wu Y L, Kong J, Gu J W. Enhanced thermal conductivities and decreased thermal resistances of functionalized boron nitride/

polyimide composites. *Compos Part B: Eng* **164**: 732–739 (2019)

[47] Wang H Y, Chang L, Yang X S, Yuan L X, Ye L, Zhu Y J, Harris A T, Minett A I, Trimby P, Friedrich K. Anisotropy in tribological performances of long aligned carbon nanotubes/polymer composites. *Carbon* **67**: 38–47 (2014)

[48] Keusch S, Haessler R. Influence of surface treatment of glass fibres on the dynamic mechanical properties of epoxy resin composites. *Compos Part A: Appl Sci Manuf* **30**(8): 997–1002 (1999)

[49] Li F, Qu C B, Hua Y, Xiao H M, Fu S Y. Largely improved dimensional stability of short carbon fiber reinforced polyethersulfone composites by graphene oxide coating at a low content. *Carbon* **119**: 339–349 (2017)

[50] Yuan J Y, Zhang Z Z, Yang M M, Guo F, Men X H, Liu W M. $TiB_2$ reinforced hybrid–fabric composites with enhanced thermal and mechanical properties for high–temperature tribological applications. *Tribol Int* **115**: 8–17 (2017)

[51] Qian M B, Sun Y Q, Xu X D, Liu L N, Song P A, Yu Y M, Wang H, Qian J. 2D–alumina platelets enhance mechanical and abrasion properties of PA612 via interfacial hydrogen–bond interactions. *Chem Eng J* **308**: 760–771 (2017)

**Junya YUAN.** He received his bachelor degree in 2014 from Henan University of Science and Technology and Ph.D. degree in 2019 from Lanzhou Institute of Chemical Physics, Chinese Academy Science. After that, he worked as an assistant researcher in the State Key Laboratory of Solid Lubrication at Lanzhou Institute of Chemical Physics. His research interests include the self-lubricating polymer composites and fabric liners, etc.

**Zhaozhu ZHANG.** He is currently working as a professor at Lanzhou Institute of Chemical Physics, Chinese Academy Science. He received his Ph.D. degree from Lanzhou Institute of Chemical Physics in 1998. His current research interests cover the tribology of composite materials, designing functional surfaces with special wetting behavior, and engineering coatings for drag-reduction. He has published more than 160 papers in important journals and gained a number of national scientific awards.

**Wei JIANG.** She is an associate researcher at Lanzhou Institute of Chemical Physics, Chinese Academy of Sciences. She obtained her bachelor degree from Beijing University of Chemical Technology in 1999. Her research area mainly focuses on the tribology design of self-lubricating fabric liners.